Българска академия на науките. Bulgarian Academy of Sciences
Аерокосмически изследвания в България, 7. Aerospace Research in Bulgaria, 7
София . 1991 . Sofia

Electron density profiles and radiowave absorption modelling in the ionospheric D-region

P. I. Vellinov, V. A. Vlaskov, N. V. Smirnova**
O. F. Ogloblina, Chr. Spasov***

Solar-Terrestial Research Laboratory, Bulgarian Academy of Sciences, Sofia
**Polar Geophysical Institute, USSR Academy of Sciences, Murmansk*
***Institute of Geophysics, Bulgarian Academy of Sciences, Sofia*

1. Introduction

The ionospheric D-region situated in the altitudinal interval 50-90 km influences considerably the radiowave propagation in a wide frequency range: very long (VLW), long (LW), middle (MW) and short (SW) waves included. In this respect of great importance is the problem of such modelling which will adequately describe the distribution of the basic parameters, determining the character of radiowave propagation and, above all, the behaviour of the basic ionosphere parameter — the electron concentration N under different conditions and states of the solar-terrestrial relationships. Such a model should define the $N(h)$-profiles dependency on the solar activity, season, time, the geographical situation, the level of magnetic, ionospheric and meteorological disturbances or, in other words, all factors influencing the character of the $N(h)$ distribution in the D-region. This is necessary for the improvement of the radiowave propagation forecast methods and the practical support of radiolinks. For this purpose a theoretical quadri-ionic model has been developed [1, 2, 6], which proved more reliable than the empirical models [7, 8], and, compared to the detailed schemes, e. g. [9, 10], has the advantage of simplicity and greater speed of calculation.

The purpose of the present work is to test the developed theoretical model [1, 2, 6] on a considerable bulk of experimental data, as well as to demonstrate the possibilities of the model to describe the various disturbed conditions in the ionosphere (polar cape absorption PCA, auroral absorption PAA, winter anomaly WA, post-storm effect PSE, etc.), as well as to continue our previous studies [11, 12].

2. Fine structure of $N(h)$-profiles modelling

An important characteristic of the $N(h)$-profiles is their shape, i. e. their non-monotonousness, presence of extrema — maximums and minimums of electron density and their heights, as wel as the gradient value dN/dh. Herewith, we are going to distinguish between two altitude regions in the D-regions: under and above 75 km. First, we are going to consider experimental data, and then the possibilities of the different models to explain the peculiarities of the profiles in both altitude intervals.

2.a. 60-75 km region modelling

For this region rocket measurements give predominantly monotonous profiles lacking in expressed minimums and maximums of N. The profiles obtained through cross-modulation display an expressed minimum at about 70 km height and a growing value of N at 60-65 km height, the same being interpreted as "cosmic ray layer" (CR-or C-layer) in the low ionosphere [3]. The model profiles formed on the basis of data concerning VLW, LW and MW propagation do not offer a single solution for the profile character under 75 km. For example, in models [3, 13, 14] the C-layer at 60-65 km is present and at 68-70 km a minimum is observed.

But, the model profiles [4, 15] (the last are obtaind using data about radio paths in the frequency range from 16 kHz to 2,5 MHz) are monotonous. Furthermore, the calculations in [16] showed that the use of the IRI-79 model [7] — a smooth profile extrapolation under 70 km, and the model [14] with a C-layer model demonstrate different VLW reflection coefficients within the frames of accuracy measurement of these parameters. The electron concentration variation 10 times in the 51-61 km interval leads to variation only in separate components in the reflection coefficient matrix. It came out that reliable conclusions concerning the N value for the low D-region can be made measuring all four components of the reflection coefficient matrix components, while in practice only one or two parameters are measured.

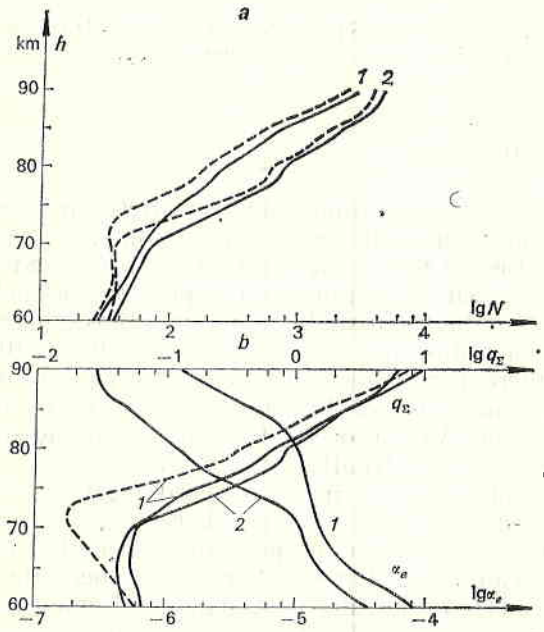

Fig. 1. Electron concentration profiles N *(a)*, electron production rate q_Σ and the effective recombination coefficient α_e *(b)* under summer *(1)* and winter *(2)* conditions: $X=78{,}5°$, $F_{1,07}=200$
———calculations taking into account electron precipitation; — — — without taking into account the particles

Now we are going to consider the profiles obtained in our theoretical model [1, 2, 6] under quiet summer and winter conditions at latitude 50°N; solar zenith angle

$X = 7{,}85°$; and high solar activity $F_{10{,}7} = 200$. These $N(h)$-profiles are presented in Fig. 1. The profiles designated by dotted line demonstrate an expressed minimum at height 72 km in summer and 70 km in winter. This minimum is received from the electron production rate q minimum (Fig. 1) as a result of: a) galactic cosmic rays ionization drop with height, and b) low intensity of the Ly-alpha line on these heights, which is nearly absorbed by the atmosphere [3]. The profiles designated by an uninterrupted line are of monotonous character. They are obtained taking into account the additional ionization source: the precipitating high-energy electrons. The background fluxes data under quiet conditions deffers considerably. In our calculations minimal values of ionization rate of that source are used from available data. It should be noted that the consideration of the additional ionization source is substantial only for adequately high values of X. At $X < 70°$ the solar radiation ionization exceeds the electron precipitation ionization to such an extent, that the monotonous growth of $N(h)$ with the altitude is provided even without counting this additional source.

2.b. Modelling of the region above 75 km

Rocket experiments and partial reflection method measurements give electron density profiles with large gradient dN/dh at altitudes 80-85 km. The cross-modulation method using the new way for obtaining N from experimental data results in an insignificant N gradient, not observed in profiles obtained untill 1971-1972. The height of that gradient and its value change in dependence with the observation conditions: in summer at middle latitudes under daytime quiet conditions 83-85 km, about 87 km at high latitudes, and up to 90 km when noctilusceni clouds are observed; in winter under normal conditions 82 km, in winter anomaly 77 km (and even 72 km); at night the gradient height is greater as compared to day values (up to 90-92 km) and is marked by a drastic fall under disturbed conditions.

Let us consider the possible reasons for the occurence of that gradient of N on the basis of the ionization balance equation [3]

$$q_\Sigma = \alpha_e N^2, \quad \alpha_e = (1 + \lambda)(\alpha_d + \lambda\alpha_i).$$

It can be supposed that dN/dh occurs either as a result of the growth in ionization rate q or due to the effective recombination coefficient change.

The calculations show a comparatively smooth total electron production rate q_Σ profile above 70 km (Fig. 1*b*). At the same time, the available ion composition mass-spectrometer measurements in the D-region (about 40 rocket experiments) show a coincidence between the gradient N height and the h_p-height, changing abruptly its prevailingly positive ion composition: from cluster ions $H^+(H_2O)$ below the transition level height h_p to simple molecular ions NO^+, O_2^+ above h_p. Let us remind that subject of discussion are altitudes above 70 km, where the negative ions are comparatively small in number ($\lambda < 1$) and the value of α_e is determined by positive ions composition:

$$\alpha_e = \alpha_d = \frac{\alpha(NO^+, O_2^+) + f^+\alpha(Cl^+)}{1 + f^+},$$

$$\alpha(NO^+, O_2^+) = 2 \cdot 10^{-7} \text{ cm}^3 \cdot \text{s}^{-1},$$

$$\alpha(Cl^+) \approx (2 \div 10) \cdot 10^{-6} \text{ cm}^3 \cdot \text{s}^{-1},$$

$$f^+ = \frac{[Cl^+]}{[NO^+] + [O_2^+]}.$$

Table 1

Conditions	Height h_p, km			
	experiment			model [1, 2, 6]
	$f^+=0,1$	$f^+=1$	$f^+=10$	
	Summer, daytime			
Equator	84,5	82,5	76,5	
Middle latitudes	87	85	80	85,5 ($X=28°$)
High latitudes	89	87	83,5	88
	Winter, daytime middle latitudes			
Quiet conditions	—	—	—	82
Winter anomaly	79	77	75	76—77
Strong anomaly	75	72	—	72
	Winter high latitudes			
Night, quiet cond.	94	92	85	>90
Night, weak PAA	86	82,5	75	82
Day/night PCA	76	72,5	69	73

The greatest changes of α_e are caused by the ion content change, corresponding to the h_p transition from $f^+=1$ to $f^+=0,1$. As shown in Table 1 [17] where mass-spectrometer measurements data are summarized, such a change of f^+ takes place in an interval about 2 km. This causes the reduction of α_e five times from $1,6.10^{-6}$ to 3.10^{-7} $cm^3.s^{-1}$, while the transition of $f^+=10$ to $f^+=1$ reduces α_e only 1,5-3 times and this process takes place in an interval of about 5-6 km. Thus, in an interval of 2 km of the transition height (equal to the N gradient height) the electron density should grow 2,3 times only due to the decrease of α_e.

3. Winter profiles modelling

Let us begin with the model $N(h)$-profiles. Fig. 2 (dotted line) shows the profiles [18] obtained following data of radiowaves propagation in a wide frequency range from 50 kHz to 2,75 MHz under low solar activity $F_{10,7}=70$, latitude 50°N, $X=78,5°$. The summer profile *1* features a small N gradient at altitudes above 85 km. But the winter profile *2* is characterised by a rather high gradient at altitudes of 82-85 km (N changes 7 times). Also, in Fig. 2 the $N(h)$-profiles calculated on the basis of the theoretical model under the same latitude conditions, zenith solar angle and solar activity (uninterrupted line) are compared. A good correspondence between the summer profiles obtained using the theoretical model and the model [18] is noticed, while the winter profiles differ considerably: our profiles under quiet conditions feature a comparatively small N gradient.

The absence of a marked N and α_e gradient in our model profiles is explained by the fact that, when calculating N with step in height 1 km, all input parameters — temperature, density and concentration of the minor neutral constituents — were given with smooth approximation of their model values, which are given, as a rule, with step in height 5 km (e. g. the CIRA —

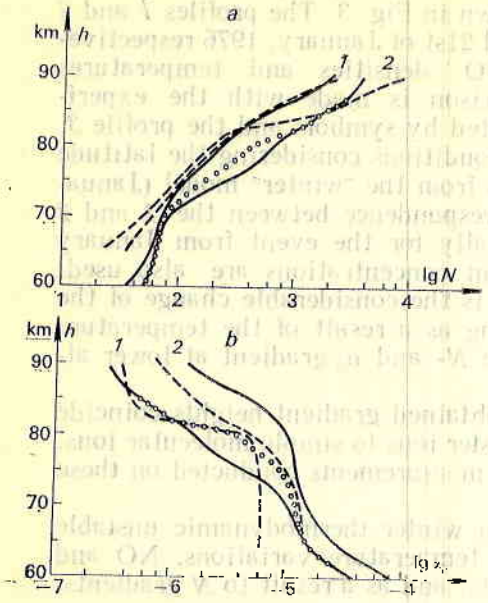

Fig. 2. Water vapours concentration influence on the $N(h)$-profiles *(a)* and $\alpha_e(h)$-profiles *(b)* under summer *(1)* and winter *(2)* conditions
———calculation for constant $k=5.10^{-6}$; ○— for $k=5.10^{-6}$ (under 80 km) and $k=1.10^{-6}$ (over 80 km); — — — model [18]

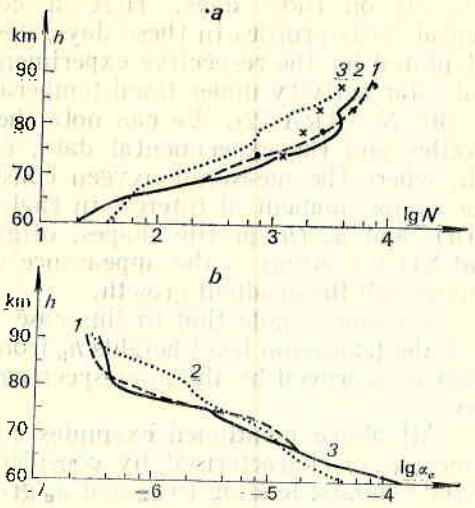

Fig. 3. $N(h)$-profiles *(a)* and $\alpha_e(h)$-profiles *(b)* under normal *(3)* and anomalous *(1, 2)* winter conditions
1 — WA 4. 01. 1976; *2* — WA 21. 01. 1976; *3* — normal day, $X=66°$
·——·, —·—·—, . . . model calculations; ●, x — experimental

72 model). The testing of the model by unit points demonstrates a relatively true representation of the transition level heights h_p from cluster to simple ions (Table 1) and of the altitude distribution of α_e and f^+ under different geophysical conditions. It is obvious that the considerable gradients of α_e, f^+ and, consequently, the N gradient occur as a result of the gradients presence in the distribution of the minor constituents, which are influenced most strongly by the dynamic processes. These neutral constituents include: H_2O, NO, O.

The influence of the H_2O gradient at altitudes 80-82 km on the $N(h)$- and $\alpha_e(h)$-profiles can be followed in Fig. 2. Let us compare the winter profiles *2*, designated by an uninterrupted line and circles. The first profile is obtained at a constant mixing coefficient $k=[H_2O]:[M]=1.10^{-6}$ along the whole altitude interval; the second — at a drastic coefficient change from $k=5.10^{-6}$ (at $h=80$ km) to 1.10^{-6} over 80 km. In the last case a considerable N gradient is obtained and the α_e profile approximates the values [18] following data concerning LW propagation. The k coefficient profile used corresponds according to [19] to a transition from turbulence absence regime in the layer under 80 km (summer conditions) to strong diffusion over 82 km (winter conditions). As it is known, the winter atmosphere is characterised by dramatic dynamic and thermal regime variations. This leads to considerable variations of N and the short-wave absorption under equal solar activity and solar zenith angle conditions. This is proved by the winter anomaly phenomenon of short-wave absorption. The electron concentration enhancement causing unusually high radiowave absorption during WA is due to ionization rate growth as a result of ionizing component NO growth and α_e decrease under higher

neutral gas temperatures. The influence of these two input parameters on the shape of the $N(h)$-and $\alpha_e(h)$-profiles is shown in Fig. 3. The profiles *1* and *2* for the anomalous winter days of the 4th and 21st of January, 1976 respectively are calculated using the measured NO densities and temperatures [20, 21] on those days. Here a comparison is made with the experimental $N(h)$-profiles in these days, designated by symbols and the profile *3*, calculated for the respective experimental conditions considering the latitude and solar activity under fixed temperatures from the "winter" model (January, 40° N, CIRA-72). We can note the correspondence between the *1* and *2* profiles and the experimental data, especially for the event from January 4th, where the measured oxygen constituent concentrations are also used. The major moment of interest in that case is the considerable change of the $N(h)$- and α_e (h)-profile shapes, originating as a result of the temperature and NO variations – the appearance of the N- and α_e-gradient at lower altitudes and the gradient growth.

We should note that in this case the obtained gradient heights coincide with the transition level heights h_p from cluster ions to simple molecular ions. That is approved by the mass-spectrometer measurements conducted on these days.

All above mentioned examples concern winter thermodynamic unstable atmosphere, characterised by considerable temperature variations, NO and water vapours, leading to q_Σ and α_e gradients, and as a result to N gradients.

4. Summer profiles modelling

Quite different is the situation in the summer upper atmosphere. Then the adequately stable thermodynamic regime ensures relative stability of the height distributions of minor neutral constituents. Besides, under low summer temperatures in the mesosphere the ion-molecular processes system acts in

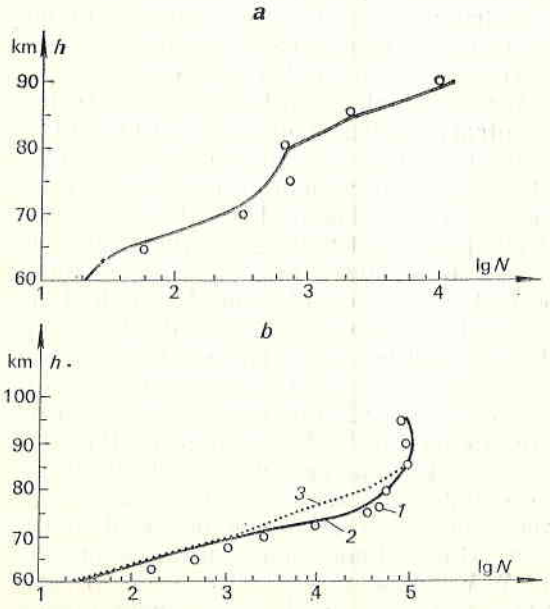

Fig. 4 $N(h)$-profiles under different conditions
a — summer daytime conditions, X=38°; ——— model calculation, O — experiment on 23. 07. 1970, Sardinia island; *b* — hight auroral absorption; *1* — experiment, *2* — model calculations under high [O], *3* — calculations under low [O]

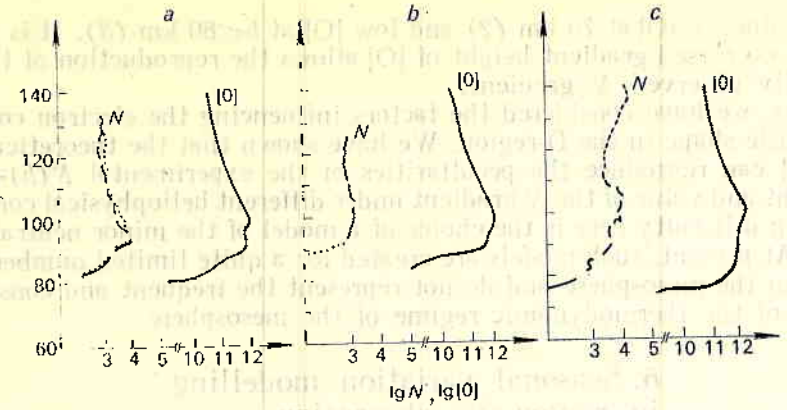

Fig. 5. Simultaneous measurements of $[O](h)$ and $N(h)$-profiles under night conditions
a — 1. 04. 1974, $X=114{,}6°$; *b* — 8. 09. 1975, $X=117°$; *c* — 7. 02. 1977, $X=126°$

such a way that neither the small temperature variations up to $\pm$ 20 K, nor the water vapour concentration influence considerably the cluster ion formation rate, and hence they do not influence the N and α_e values. These two factors explain the absence of marked N fluctuations in the quiet summer ionosphere under equal heliogeophysical conditions and the great smoothness of the summer $N(h)$-profiles as compared to the winter ones. This can be illustrated by Figs 2 and 4. For example, in Fig. 4*a* a $N(h)$-profile is shown measured in the summer middle-latitude ionosphere (designated by circles) and a profile calculated for the same conditions (uninterrupted curve) form our model. The experiment was conducted on July 23rd, 1970 in Sardinia, at $X=38°$.

5. Night profiles modelling

Here, the basic factor, determining the $N(h)$-profile shape under quiet conditions is the atomic oxygen height distribution $[O](h)$. As it is evident from the results obtained by the synchronous $N(h)$ and $[O](h)$-profiles measurements and in Soust Wist (57° N) — Fig. 5*a*, *b*, *c* [22], the electron density sharp gradient height (75-85 km) coincides with the sharp growth height [O]. The atomic oxygen concentration under night conditions at 75-85 km height can variate up to 3 orders. In the night period (unlike the day period) the $[O](h)$-profile is determined mainly by the dynamic processes. Then, a threefold change of the turbulent diffusion coefficient leads to growth of [O] with more than an order for 75 km [23]. Even greater changes of [O] — up to three orders — are obtained for the same height in the calculations [19], exclusively owing to changes of the dynamic regime.

The second factor causing the atomic oxygen concentration increase in the night high-latitude mesosphere can be the precipitation of the high-energy particles. According to calculations [5] under a night disturbance with duration 1 hour, the atomic oxygen concentration grows 10^5 times at $h=60$ km and 10^2 times at $h=70$ km. The influence of the growth of [O] during the night disturbance on the $N(h)$-profile shape can be seen in Fig. 4*b*. Here, a comparison is made between the experimental profile *(1)* of the night auroral absorption on February 21st, 1976 in Kiruna [24], and the profiles calculated with

higher values of [O] at 75 km *(2)* and low [O] at $h<80$ km *(3)*. It is evident, that the decreased gradient height of [O] allows the reproduction of the experimentally observed N gradient.

Thus, we have considered the factors influencing the electron concentration profile shape in the D-region. We have shown that the theoretical model [1, 2, 6] can reproduce the peculiarities of the experimental $N(h)$-profiles: the height and value of the N gradient under different heliophysical conditions. The main difficulty here is the choice of a model of the minor neutral constituents. At present, such models are created for a quite limited number of conditions in the mesosphere and do not represent the frequent and considerable changes of the thermodynamic regime of the mesosphere.

6. Seasonal variation modelling in radiowave absorption

Now, on the basis of our theoretical model we are going to try to reproduce and explain the seasonal variations in the radiowave absorption L. As it has been established during the observations of long standing, for the middle

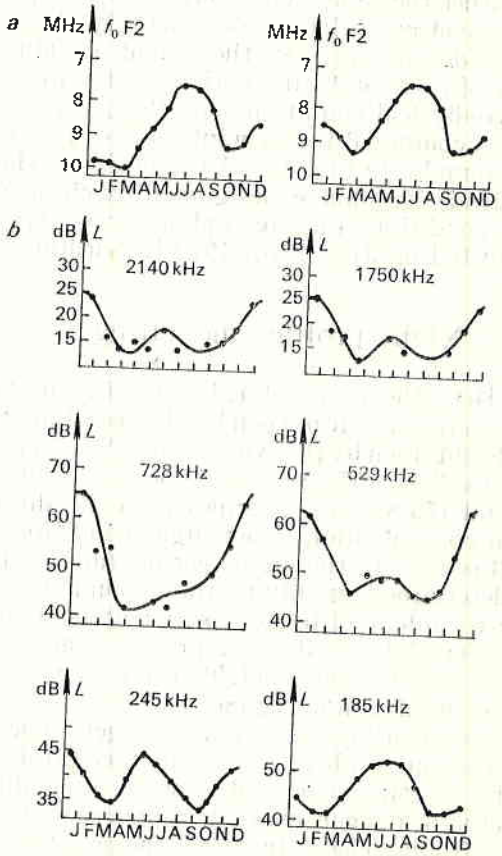

Fig. 6. Seasonal variations of critical frequencies f_0F2 of the F2 layer *(a)*, and L absorption under various frequencies *(b)*.

latitude LW, MW and SW paths (using the methods A3 and A1), the monthly median absorption values at constant solar zenith angle X have a half-year variation with a minimum in the equinox months and a maximum in the solstice periods (Fig. 6) [18]. At the same time, in the SW range the greatest maximum is observed in winter (WA) and in LW — in (summer anomaly — SA). At the top of Fig. 6 the season variations of the maximum median critical frequencies f_0F2 under moderate solar activity for 1971-1972 and 1983 are shown and the mean f_0F2 values for the whole period of observation (1962-1983), following data of the Sofia ionospheric station. As a whole, f_0F2- and L-courses are reverse, illustrating the synchronous seasonal redistribution of the electron concentration between the upper and the lower ionosphere, depending on solar activity too.

6.a. Winter anomaly in short-wave absorption

The essence of this phenomenon is that the short waves absorption L under equal conditions (solar activity and X) in winter is greater than in summer. This is the regular WA. But in certain days or groups of days (e. g. the discussed above events from 4th and 21st January, 1976) the absorption grows considerably even in comparison with the mean winter absorption of the WA. These are the anomaly days of the WA, or the so called anomalous WA. As the electron concentration is the basic parameter determining the radiowaves absorption value (predominantly non-deviating in the D-region and deviating in the E-layer), the above mentioned absorption variations winter-summer and during WA (normal and anomalous) are caused by the respective N variations at altitudes 75-80 km.

The calculations using the theoretical model [1, 2, 6] were conducted under equal winter and summer $[NO](h)$-profiles; neutral gas temperature and density values are taken from the CIRA-72 model for the months January and July, for latitudes 40° and 50° N, corresponding to the middle radiowaves reflection point of the used for comparison nine middle-latitude paths [6].

The calculated relations of the winter-to-summer absorption under low solar activity, $X=60°$ ($\cos X=0{,}5$) and $X=78{,}5°$ ($\cos X=0{,}2$) for the two models of $[H_2O](h)$-distributions are presented in Table 2. It illustrates the correspondence between experimental data and the results from the theoretical model. The greater values of winter absorption as compared to summer results from the correspondingly greater winter N than the summer ones (Fig. 2). The latter is determined by the fact that under high winter mesosphere temperatures the formation rate of a quickly recombinating cluster ions rate is smaller than under lower summer temperatures, hence the α_e value is smaller. Present results enrich and summarize our initial quantitative estimation of WA, obtained in [11, 12].

Table 2

$[H_2O]_w$	$[H_2O]_s$	L_w/L_s	
		40°N; $\cos X=0{,}5$; $X=60°$	50°N; $\cos X=0{,}2$; $X=78{,}5°$
1.10^{-6}[M]	1.10^{-6}[M]	1,5	1,8
1.10^{-6}[M]	5.10^{-6}[M]	2,0	2,2

In that case, under low equivalent frequencies $f_1 = f \cos i$ <100 kHz the radiowave absorption is deviating in the D-region and is determined by the electron density gradient and the collision frequency of the reflecting layer. We have calculated the profiles for latitudes 40° and 50° N, X=66° and 78,5° for low $F_{10,7}$=70 and high $F_{10,7}$=200 solar activity (Figs 1-3).

For determining the reflecting layer height of the path Allouis-Sofia 164 kHz/1720 km, the electron concentration necessary for reflection was determined for a collision frequency profile given as $\nu\ (h) = 6{,}3.10^5\ p(h)$, where p is the pressure, N/m². The results from the calculation of the winter-to-summer absorption relation L_s/L_w and the reflection heights are shown in Table 3, and experimental data for L_s/L_w in the period 1977-1981 are given in Table 4. It can be noted that the calculated summer absorption excess over the winter absorption for LW is in reasonable correspondence with experimental data. The received seasonal variations in reflecting layer height (h_r in summer are 3 km higher than in winter) and the reflecting layer rising with the solar activity decrease also corresponds to experimental data [25]. As our model calculations show, the summer absorption excess of LW over the winter absorption results from the smaller dN/dh gradient in summer, as compared to winter.

Table 3

Latitude N	$F_{10,7}$	X	$\frac{L_s}{L_w}$	Height, km	
				summer	winter
40°	200	66°	1,55	74,3	71,6
	70		1,4	75	72,5
50°	200	78,5°	1,7	77,5	74
	70		2,0	78,3	74,5

Table 4

X	L_s/L_w					
	1977	1978	1979	1980	1981	Average
66°	2	1,4	1,8	1,77	1,5	1,7
78,5°	2	1,4	1,9	1,8	1,45	1,7

7. Conclusion

The test of the theoretical quadri-ionic model of the D-region [1, 2, 6] conducted in the present work over a large bulk of the *in situ* and ground-based data shows that it represents experimental data with greater precision, as compared to the existing empirical models for the $N(h)$-profiles and for the radiowaves absorption L in various frequency ranges. For example, describing the seasonal L variations, the IRI-79 model [7] gives higher values for the LW absorption in winter, and lower values for SW. Thus, neither the observed values of WA at high frequences nor the SA at low frequences can be reproduced. Our theoretical model explains the seasonal variations of N (normal WA constituent) and the separate strong variations dN/dt in winter (anomalous

WA constituent) by means of seasonal and non-regular temperature and minor neutral constituents variations in winter. But that model describes quantitatively all other ionospheric disturbances and anomalies (PCA, PAA, PSE, etc.), if the respective input parameters are known. This proves the adequately precise counting of the hybrid quadri-ionic scheme [1, 2, 6] of the basic processes and dependencies from the control parameters T, $[H_2O]$, $[O]$, etc. as it is in the detailed schemes [9, 10]. The advantages of the quadri-ionic scheme are in the simpler calculations, while the computations following detailed schemes require considerable amount of machine time, leading to more difficult input parameters variation necessary for the different ionosphere disturbances modelling. It is clear that at present the ionization-recombination cycle of the theoretical model is well balanced and the focus of study will pass to the investigation of such parameters as the concentration of minor neutral constituents, corpuscule sources of ionization (especially at high latitudes), variations of the composition and temperature of the basic atmosphere components and a specification of the CIRA-72 model.

References

1. Смирнова, Н. В., В. А. Власков. Препринт ПГИ 82-3-17. Апатиты, КФ АН СССР, 1982, с. 46.
2. Смирнова, Н. В., О. Ф. Оглоблина, В. А. Власков. Препринт ПГИ 84-08-36. Апатиты, КФ АН СССР, 1984, с. 31.
3. Веллинов, П. И., Г. Т. Несторов, Л. И. Дорман. Воздействие космических лучей на ионосферу и распространение радиоволн. С., БАН, 1974.
4. Красиушкин, П. Е., Т. А. Князева. — Геомагнетизм и аэрономия, **10**, 1970, № 6, с. 993.
5. Смирнова, Н. В., С. И. Козлов, В. А. Власков, Н. А. Овчинников. — Космические исследования, **12**, 1984, № 4, с. 565.
6. Vellinov, P. I., N. A. Smirnova, V. A. Vlaskov. — Adv. Space Res., **4**, 1984, No 1, p. 123.
7. International Reference Ionosphere — IRI-79, World Data Center A, Report UAG-82, Boulder/Colorado, 1981.
8. McNamara, L. F. — Radio Sci., **14**, 1979, No 6, p. 1165.
9. Reid, G. C. — Planet. Space Sci., **25**, 1977, p. 257.
10. Torkar, K. M., M. Friedrich. — J. Atmosph. Terr. Phys., **45**, 1983, No 6, p. 369.
11. Smirnova, N. V., V. A. Vlaskov, P. I. Vellinov. — Compt. rend. Acad. bulg. Sci., **36**, 1983, No 10, p. 1307.
12. Vellinov, P. I., V. A. Vlaskov, N. A. Smirnova. — Compt. rend. Acad. bulg. Sci., **36**, 1983, No 1, p. 73.
13. Deeks, D. G. — Proc. Roy. Soc., **A 291**, 1966, p. 413.
14. Bain, W. C., M. D. Harrison. — Proc. IEE, 1972, No 7, p. 790.
15. Bremer, J., W. Singer. — J. Atmosph. Terr. Phys., **39**, 1977, No 1, p. 25.
16. Ramanamurty, Y. V. — Adv. Space Res., **2**, 1983, No 10, p. 205.
17. Kopp, E. — Invited Review Paper 7.4.7. COSPAR, Budapest, 1980.
18. Bremer, J., K. Evers, J. Taubenheim. — Gerlands Beitr. Geophysik, **90**, 1981, No 4, p. 296.
19. George, J. D., S. P. Zimmerman, T. J. Keneshea — Space Res., **12**, 1972, p. 695.
20. Beran, D., W. Bangert. — J. Atmos. Terr. Phys., **41**, 1979, p. 1091.
21. Becker, M., J. Bate et al. — J. Atmos. Terr. Phys., **41**, 1979, p. 1075.
22. Dickinson, P. H. G., W. C. Sain et al. — Proc. Roy. Soc., **A 369**, 1980, p. 379.
23. Keneshea, T. J., S. P. Zimmerman, C. R. Philbrick. — Planet. Space Sci., **27**, 1979. No 4, p. 385.
24. Bjorn, L. G., F. Arnold, D. Krankowsky et al. — J. Atmos. Terr. Phys., **41**, 1979, No 12, p. 1185.
25. Lauter, E. A., J. Taubenheim, G. Entzian et al. — HHI-STP-Report, **7**, 1976, p. 83.

Моделирование профилей электронной концентрации и поглощения радиоволн в D-области ионосферы

П. И. Велинов, В. А. Власков, Н. В. Смирнова, О. Ф. Оглоблина, Хр. В. Спасов

(Резюме)

На основе разработанной теоретической модели D-области ионосферы, включающей четыре положительных и отрицательных иона и электроны, смоделирована тонкая структура профилей электронной концентрации (форма профиля, его немонотонность, наличие максимумов и минимумов N и их высоты, наличие градиентов dN/dh). Выделены две области высот: ниже и выше 75 km. Показаны возможности моделей по воспроизведению и объяснению особенностей профилей в этих двух высотных интервалах в дневных и ночных условиях в зависимости от сезона. На основе теоретической модели также объяснены сезонные вариации поглощения L радиоволн: зимняя аномалия поглощения коротких волн и летняя аномалия поглощения длинных волн.